IEEE Access
Multidisciplinary | Rapid Review | Open Access Journal

Received 17 February 2023, accepted 18 March 2023, date of publication 21 March 2023, date of current version 30 March 2023.

Digital Object Identifier 10.1109/ACCESS.2023.3260146

RESEARCH ARTICLE

0.5 V Multiple-Input Multiple-Output Differential Difference Transconductance Amplifier and Its Applications to Shadow Filter and Oscillator

FABIAN KHATEB[1,2,3], MONTREE KUMNGERN[4], TOMASZ KULEJ[5], AND RAJEEV KUMAR RANJAN[6], (Senior Member, IEEE)

[1]Department of Microelectronics, Brno University of Technology, 601 90 Brno, Czech Republic
[2]Faculty of Biomedical Engineering, Czech Technical University in Prague, 272 01 Kladno, Czech Republic
[3]Department of Electrical Engineering, University of Defence, 662 10 Brno, Czech Republic
[4]Department of Telecommunications Engineering, School of Engineering, King Mongkut's Institute of Technology Ladkrabang, Bangkok 10520, Thailand
[5]Department of Electrical Engineering, Czestochowa University of Technology, 42-201 Czestochowa, Poland
[6]Department of Electronics Engineering, IIT (ISM) Dhanbad, Dhanbad 826004, India

Corresponding author: Montree Kumngern (montree.ku@kmitl.ac.th)

This work was supported by the University of Defence, Brno, within the Organization Development Project VAROPS.

ABSTRACT This paper presents new applications of low-voltage and low-power multiple-input multiple-output differential difference transconductance amplifier (DDTA). The multiple-input bulk-driven MOS transistor (MIBD MOST) technique provides multiple-input of the active device that simplifies the application's topology and reduces its power consumption. The proposed DDTA has been used to realize multiple-input single-output shadow filter. Both voltage- and transimpedance-mode filtering functions can be obtained. The natural frequency and the quality factor of the shadow filter can be independently and electronically controlled using DDTA-based amplifiers. The proposed shadow filter has been modified to work as a shadow oscillator. The condition and frequency of oscillation can be controlled independently and electronically. The DDTA is capable to work with 0.5V supply voltage and consumes 218.2 nW. The applications have been designed and simulated in Cadence using 0.18μm TSMC CMOS technology.

INDEX TERMS Differential difference transconductance amplifier (DDTA), shadow filter, shadow oscillator, analog filter, low-voltage, low-power CMOS.

I. INTRODUCTION

Universal filters are the analog signal processing circuits that usually provide several filtering responses into single topology such as low-pass (LP), high-pass (HP), band-pass, band-stop (BS), and all-pass (AP) filters. They can be realized based on voltage-mode or current-mode techniques. The active devices that provide multiple-input voltage terminals bring realization benefits to voltage-mode filters while the active devices that provide multiple-output current terminals bring realization benefits to current-mode filters. This work is focused on the voltage-mode filter, realized using multiple-input multiple-output active device.

The associate editor coordinating the review of this manuscript and approving it for publication was Ludovico Minati.

Considering the input and output terminals of the universal filters, the universal filters can be classified into three groups. If the single signal is applied to input and variant filtering responses are obtained from its variant output terminals, it can be classified as single-input multiple-output (SIMO) universal filter [1], [2], [3], [4]. If the filtering responses are obtained from single output terminal and the signals are selected to apply to variant input terminals, it can be classified as multiple-input single-output (MISO) universal filter [5], [6], [7], [8], [9]. If input signals are selected to apply to variant input terminals and the variant filtering responses are obtained from variant output terminals, it can be classified as a multiple-input multiple-output (MIMO) universal filter [10], [11], [12]. Compared with MISO and MIMO filters, SIMO filter usually requires maximum number of

active devices. The active devices that provide multiple-input voltage terminals like differential difference current conveyor (DDCC) [13] and fully differential second-generation current conveyor (FDCCII) [14] are most suitable for realizing voltage-mode MISO and MIMO filters, while the active devices that provide multiple-output current terminals such as multiple-output second-generation current conveyor (CCII) [15] and multiple-output operational transconductance amplifier (OTA) [16] are most suitable for realizing current-mode MISO and MIMO filters.

For realization of analog filters, the natural frequency and the quality factor are important parameters that usually depend on internal elements of the filters such as resistances, transconductances or capacitances. For integrated circuits, the tuning ability is required to set the demanded natural frequency and the quality factor of the filter application and to readjust any possible parameters' deviation, caused by the process voltage and temperature variations. Moreover, tunable filters are required in the bio-signal processing area and communication systems [17], [18], [19]. Usually, many universal filters have the possibility to tune the natural frequency and the quality factor via the circuit components such as resistance, transconductance, and capacitance [1], [2], [3], [4], [5], [6], [7], [8], [9], [10], [11], [12]. Unfortunately, tuning the natural frequency and the quality factor via the circuit components will affect the filters performance.

New techniques to tune the natural frequency and the quality factor, the so-called shadow filter or agile filter, have recently been proposed [20], [21], [22]. The concept of this technique is to use external amplifiers to tune the natural frequency and the quality factor of filters. Thus, the circuit components of the core filter are not changed. The systems in [20], [21], and [22] are suitable for realizing SIMO shadow filters. The system that is suitable for realizing MISO shadow filters has been proposed in [23]. Based on the systems in [20], [21], [22], [23], several shadow filters of agile filters have been proposed based on current-mode approaches [24], [25], [26], [27], [28], [29], [30], [31] and voltage-mode approaches [32], [33], [34], [35], [36], [37], [38], [39], [40], [41], [42], [43], [44].

Considering the voltage-mode filters in [32], [33], [34], [35], [36], [37], [38], [39], [40], [41], [42], [43], and [44], on which this work focuses, the shadow filters, in [33] uses 5-CFOAs (current-feedback operational amplifier), 9-R (resistor), 2-C (capacitor), and in [34] uses 4-CFOAs, 7-R, 2-C. However, the filters in [33] and [34] provide only band-pass (BP) filtering response. The shadow filters that offer low-pass (LP) and BP filtering responses have been proposed employing variant active and passive elements such as 3-OTRAs (operational trans-resistance amplifier), 11-R, 4-C in [32], 1-VDTA (voltage differencing transconductance amplifier), 2-C in [36], 2-VDTAs, 2-C in [37], 3-VDTAs, 2-C in [38], 4-VDTAs, 2-C in [39], 6-OTAs (operational transconductance amplifier), 2-C in [43], 3-VCIIs (second generation voltage conveyor), 6-R, 4-C in [44]. While the shadow filter in [40] employs 3-VDGAs (voltage differencing gain amplifier), 2-C, and offers LP, and high-pass (HP) filtering functions. The shadow filter in [35] employing 3-DDCCs (differential difference current conveyor), 4-R, 2-C offers LP, BP, HP filtering responses. However, this shadow filter lacks electronic tuning ability and the DDCC use 1 V of supply voltage. The shadow filter in [42] offers electronic tuning ability and offers LP, BP, HP, BS (band-stop), AP (all-pass) filtering responses. However, the active device, VDDDA (voltage differencing differential difference amplifier), that was used in [42] use ± 0.9 V of supply voltage which is not suitable for low-voltage and low-power applications. It should be noted that the shadow filters in [24], [25], [26], [27], [28], [29], [30], [31], [32], [33], [34], [35], [36], [37], [38], [39], [40], [41], [42], [43], and [44] are based on SIMO shadow filters. There is a MISO shadow filter reported in [23], but the circuit employs several CFOAs and resistors and lacks electronic tuning capability. Moreover, LP, HP, BP, BS filtering responses are not obtained from a single topology.

From the concept of DDCC in [13], this device has been developed next to obtain electronic tuning ability as differential difference current conveyor transconductance amplifier (DDCCTA) [45], and differential difference transconductance amplifier (DDTA) [46], [47]. Thus, these devices offer voltage addition and subtraction ability as first stage and electronic tuning capability as second stage. Recently, the DDTAs have been developed to operate with low supply voltage and low power consumption for applications in universal filters and oscillators [48], [49], [50]. These devices use unconventional techniques such as multiple-input MOS transistor (MOST) technique to realize multiple-input active devices such as multiple-input OTA [51]. To confirm the unconventional multiple input MOST technique is possible in the practice, it was experimentally verified in [52] and [53].

This paper presents multiple-input single-output shadow filters and oscillator using multiple-input multiple-output DDTAs. The multiple-input bulk-driven MOST technique has been used to realize multiple-input DDTA. The proposed shadow filters provide high-input and low-output impedance. The filtering functions can be easily obtained by appropriately applying the input signals. The natural frequency and the quality factor can be controlled electronically by external amplifiers. The proposed shadow filter has been also modified to work as shadow oscillator.

II. PROPOSED CIRCUIT

A. PROPOSED MULTIPLE-INPUT MULTIPLE-OUTPUT DDTA

The symbol of the MIMO-DDTA is shown in Fig. 1. In ideal case its voltage and current relationship can be expressed by:

$$\left.\begin{array}{c} V_w = V_{y+1} + \ldots + V_{y+n} - V_{y-1} - \ldots - V_{y-n} \\ I_{o1} = \ldots = I_{on} = g_m V_w \end{array}\right\} \quad (1)$$

The CMOS structure of the DDTA with two inputs and two current outputs is shown in Fig. 2. The circuit consists of two main parts, a differential-difference amplifier (DDA), that

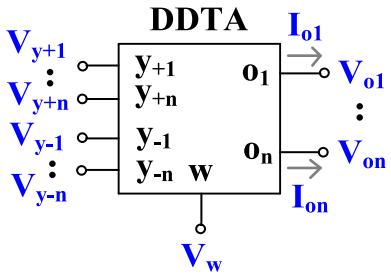

FIGURE 1. Symbol of MIMO-DDTA.

was first presented in [48] and the transconductance amplifier (TA), presented in [51] in a single input form, i.e. without multiple inputs. The DDA circuit can be seen as two-stage amplifier.

The first stage (M_1-M_{16}) is a current mirror OTA with differential-difference amplifier at the input. The input differential amplifier is based on a non-tailed bulk-driven differential pair (M_1-M_2), which is able to operate at extremely low supply voltages, while offering truly differential behavior, with good common-mode and power supply rejection ratios (CMRR and PSRR respectively). The differential-difference action is realized using multiple-input MOS transistors M_{1A} and M_{1B}. Their structure is shown in Fig. 2b. The number of inputs is increased by connecting a capacitive divider/voltage summing circuit, composed of the capacitors C_B to the bulk terminal of an MOS transistor. In order to ensure proper biasing for DC, each capacitor is shunted with a large resistance R_L, which was realized by anti-parallel connection of two MOS transistors with minimum size and V_{GS} =0. The MI-MOS transistor was experimentally verified in [52] and [53].

For frequencies much larger than $1/R_LC_L$, assuming that all the capacitances C_B are equal to each other and much larger than parasitic capacitances of MOS transistor, the AC signal at the bulk terminals of the multiple input transistors can be expressed as:

$$V_b = \sum_{i=1}^{n} \frac{V_i}{n} \tag{2}$$

where n is the number of inputs of the MI-MOS transistor. In the proposed design n = 2, thus, the AC differential voltage at the bulk terminals of the input differential pair M_{1A} and M_{1B}, V_{id} can be expressed as:

$$V_{id} = \frac{1}{2}\left\{\left(V_{y+1} + V_{y+2}\right) - \left(V_{y-1} + V_{y-2}\right)\right\} \tag{3}$$

Thus the function of a differential-difference amplifier is realized, using only one active differential pair. This allows decreasing the consumed power and simplify the overall structure of the DDA. Note, that DDA in this application operates with negative feedback, thus creating a differential-difference current conveyor. The coefficient 1/2 in (3) only affects the internal voltage gain of DDA, but the resulting DDCC realize its main function given by the first equation of (1).

Since the bulk-driven technique and the input capacitive divider lowers the voltage gain of the internal DDA, a partial positive feedback (PPF) was applied in the input stage to increase the voltage gain. The positive feedback is introduced by the cross-coupled pairs of transistors M_7-M_8 and M_9-M_{10}, which generate negative conductances, thus decreasing the total conductances seen at the drains of M_{2A}-M_{2B} and M_5-M_6 respectively, and consequently increasing the overall voltage gain of the internal DDA. Note, that two PPF circuits were applied in the proposed structure. This allows decreasing the circuit sensitivity to transistor mismatch, as compared to the structure with one PPF, while offering the same gain improvement [48]. The second stage of the internal DDA operates in class A in common source configuration. The capacitor C_C is used for frequency compensation.

The open-loop low-frequency voltage gain of the DDA, from one differential input, with the second input grounded for AC signals, can be expressed as [48]:

$$A_{vo} = \beta \cdot \frac{2g_{mb1}\left(r_{ds15}||r_{ds12}\right) g_{m16}\left(r_{ds16}||r_{ds13}\right)}{\left(1-m_1\right)\left(1-m_2\right)} \tag{4}$$

where $\beta = 1/2$ is the voltage gain of the input capacitive divider for AC signals and the coefficients m_1 and m_2 can be expressed as:

$$m_1 = \frac{g_{m9,10}}{g_{m5,6} + g_{ds2} + g_{ds3,4} + g_{ds7,8}} \cong \frac{g_{m9,10}}{g_{m5,6}} \tag{5}$$

$$m_2 = \frac{g_{m7,8}}{g_{m2} + g_{ds1} + g_{ds5,6} + g_{ds9,10}} \cong \frac{g_{m7,8}}{g_{m2}} \tag{6}$$

The coefficients m_1 and m_2 can be considered as the ratios of negative to positive conductances in "bottom" and "upper" PPF. The coefficients can range from zero (lack of positive feedback) to unity (100% positive feedback). Note, that the voltage gain tends to infinity as m_1 and/or m_2 tend to unity, however, at the cost of increased circuit sensitivity to transistor mismatch. In the proposed design $m_1 = m_2 = 0.5$, that provides improvement of the voltage gain by ca. 12 dB, while maintaining the circuit sensitivity at a moderate level.

The gain-bandwidth product of the internal DDA, which is approximately equal to the 3-dB frequency of the voltage gain of the resulting DDCC (from y_{-2} to w terminal), can be approximated as:

$$GBW = \beta \cdot \frac{2g_{mb1}}{\left(1-m_1\right)\left(1-m_2\right)C_C} \tag{7}$$

The TA block is realized using a source-degenerative BD differential pair [51]. The source degenerative transistors M_{15} and M_{16} operate in a triode region, thus increasing the linear range of the input pair by around 3 times, as compared with a classical BD pair. The bulk terminals of M_{15} and M_{16} are tied together with the bulk terminals of M_1 and M_2 respectively, which provides better immunity to common-mode signals. In the weak inversion region the optimum linearity is achieved if the following condition is satisfied [51]:

$$k = \frac{(W/L)_{15.16}}{(W/L)_{1,2}} = 0.5 \tag{8}$$

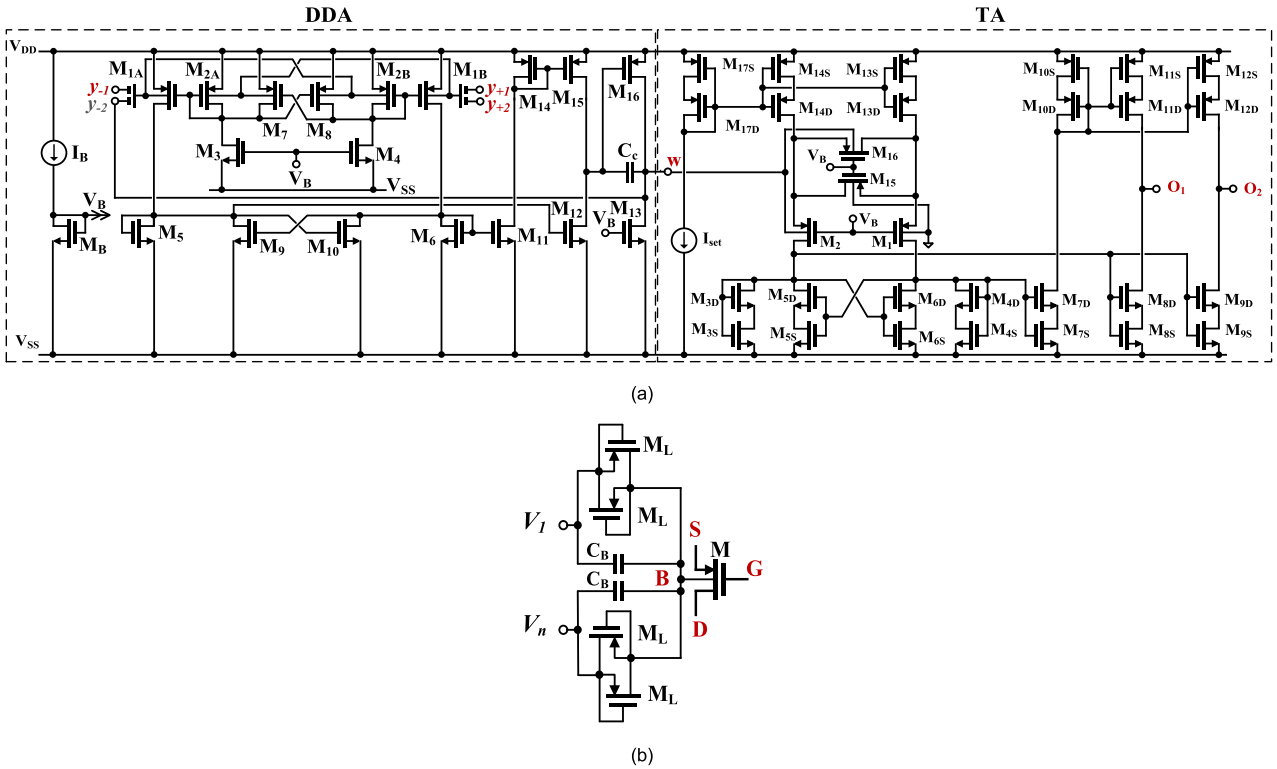

FIGURE 2. CMOS implementation of proposed MIMO-DDTA, (a) schematic, (b) MIBD MOST technique.

where W and L are the transistor channel width and length respectively.

The current mirrors used in this structure employ the so called self-cascode transistors, that allows increasing the output resistance of the OTA, and consequently its DC voltage gain, while not limiting the output voltage swing in a noticeable manner. In order to further increase the voltage gain, a PPF circuit with transistors $M_{5S,D}$, $M_{6S,D}$ has been used. Note, that the resulting conductances at the drains of M_{5D} and M_{6D} should not be too small, to prevent large voltage swing at these nodes, which could cause entering M_1 and M_2 in triode region for larger input voltages, thus limiting the circuit linearity. For optimum case (k=0.5), the circuit transconductance g_m can be approximated as:

$$g_m \cong \frac{\eta}{(1-m_3)} \cdot \frac{4k}{4k+1} \cdot \frac{I_{set}}{n_p U_T} \tag{9}$$

where $\eta = g_{mb1,2}/g_{m1,2}$ is the bulk to gate transconductance ratio at the operating point for the input transistors M_1 and M_2, $m_3 \cong g_{m5,6SC}/g_{m3,4SC}$ is the ratio of transconductances of the self cascode transistors in PPF circuit, n_p is the sub-threshold slope factor for p-channel MOS transistors and U_T is the thermal potential. Note, that the circuit transconductance can be regulated with I_{set}.

In order to limit both, the transconductance sensitivity to transistor mismatch, as well as the amplitude of the voltage swing at the drains of M_1 and M_2, the coefficient m_3 was chosen to be equal to 0.3 only. Thus, according to (9), the circuit transconductance, was increased around 1.43 times, as compared to a version without PPF. Since the branch currents of M_7, M_8 and M_9 are decreased by the ratio of $W/L_{7-9}/(W/L_{3,4}+W/L_{5,6})$, that entails decreasing the output conductance at the same proportion, the resulting voltage gain of the TA is increased by around 5.3dB, while maintaining sufficiently low sensitivity to transistor mismatch and limited voltage swing at the drains of M_1 and M_2.

The DC voltage gain of the TA can be expressed as:

$$A_{vTA} \cong g_m \left(g_{m8D} r_{ds8D} r_{ds8S}\right) || \left(g_{m11D} r_{ds11D} r_{ds11S}\right) \tag{10}$$

As mentioned previously, A_{vTA} is increased thanks to the SC connections of transistors. The proposed TA has two outputs, as required by the particular application discussed in this work. The second output (O_2) provides a copy of the current observed at the first output O_1.

B. PROPOSED SHADOW FILTER

Fig. 3 shows the block diagram of the shadow filter in [23]. It consists of one biquad filter and three amplifiers. Unlike shadow filters in [20], [21], and [22], the shadow filter in [23] realizes multiple-input single-output (MISO) biquad filter, thus the filtering responses such as LP, BP, HP, and BS can be obtained by appropriately applying the input signals. Fig. 4 shows the biquad filter employing three MIMO-DDTAs and two grounded capacitors. Thanks to multiple input of DDTA, the non-inverting and inverting versions of LP, BP, HP, and BS filtering responses can be easily obtained.

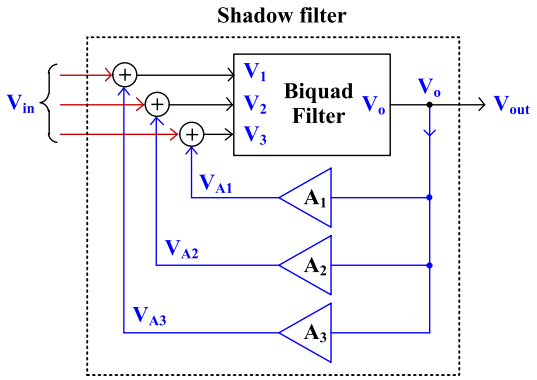

FIGURE 3. Block diagram of a shadow filter.

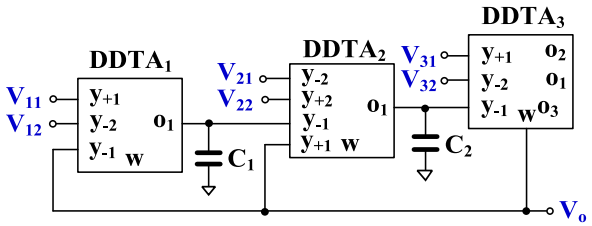

FIGURE 4. Multiple-input single-output biquad filter using MIMO-DDTAs.

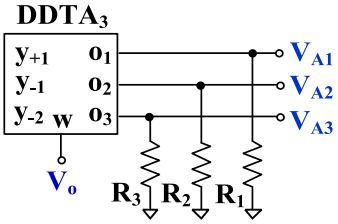

FIGURE 5. The multiple-output amplifier using MIMO-DDTA.

It should be noted that the input terminals of the filters show high-impedance level, thus they can be connected to sources without any buffer circuit. Using (1) and nodal analysis, the output voltage V_o can be expressed by, as in (11), shown at the bottom of the next page.

The non-inverting LP, BP, and HP filters can be obtained by applying the input signal to the input terminals V_{11}, V_{21}, and V_{31}, respectively, and the inverting LP, BP, and HP filters can be obtained by applying the input signal to the input terminals V_{12}, V_{22}, and V_{32}, respectively. It should be noted that node V_o shows low-impedance level.

Fig. 5 shows the multiple-output amplifier using multiple output DDTA. The circuit consists of one DDTA and three resistors. Referring to Fig. 3, the input terminal of the amplifier is V_o and the output terminals of the amplifier are V_{A1}, V_{A2}, and V_{A3}, respectively. Using (1) and nodal analysis, the voltage gains of the amplifier can be expressed by

$$A_1 = \frac{V_{A1}}{V_o} = g_{m3}R_1 \tag{12}$$

$$A_2 = \frac{V_{A2}}{V_o} = g_{m3}R_2 \tag{13}$$

$$A_3 = \frac{V_{A3}}{V_o} = g_{m3}R_3 \tag{14}$$

Thus, the voltage gains A_1, A_2, and A_3 can be controlled by resistances R_1, R_2, and R_3, respectively.

The proposed shadow filter with MISO-type filter is shown in Fig. 6. The circuit consists of the biquad filter in Fig. 4 and the amplifier in Fig. 5. It should be noted that $DDTA_3$in Fig. 4 can be used as amplifier, thus minimum active devices of the shadow filter can be obtained as in Fig. 6 (a). Using (11)-(14), the variant filtering responses of the shadow filter can be obtained as follows:

Case I

The input signal V_{in} is applied to V_{11}, input V_{12} is connected to V_{A1} (A_1), input V_{32} is connected to V_{A3} (A_3), and inputs V_{21}, V_{22}, V_{31} are connected to grounded (A_2 is not used in this case). With these assumptions, the output becomes:

$$V_{out} = \frac{s^2C_1C_2(-V_{32}) + g_{m1}g_{m2}(V_{in} - V_{12})}{s^2C_1C_2 + sC_1g_{m2} + g_{m1}g_{m2}} \tag{15}$$

Combining (12), (14), (15), the transfer function can be expressed as:

$$V_{out-LP-I} = \frac{g_{m1}g_{m2}V_{in}}{s^2C_1C_2(1 + g_{m3}R_3) + sC_1g_{m2} + g_{m1}g_{m2}(1 + g_{m3}R_1)} \tag{16}$$

The input signal V_{in} is applied to V_{31}, input V_{12} is connected to V_{A1} (A_1), input V_{32} is connected to V_{A3} (A_3), and inputs V_{11}, V_{21}, V_{22} are connected to grounded (A_2 is not used in this case). With these progresses, the output becomes:

$$V_{out} = \frac{s^2C_1C_2(V_{in} - V_{32}) + g_{m1}g_{m2}(-V_{12})}{s^2C_1C_2 + sC_1g_{m2} + g_{m1}g_{m2}} \tag{17}$$

Combining (12), (14), (17), the transfer function can be expressed as:

$$V_{out-HP-I} = \frac{s^2C_1C_2V_{in}}{s^2C_1C_2(1 + g_{m3}R_3) + sC_1g_{m2} + g_{m1}g_{m2}(1 + g_{m3}R_1)} \tag{18}$$

The input signal V_{in} is applied to V_{21}, input V_{12} is connected to V_{A1} (A_1), input V_{32} is connected to V_{A3} (A_3), and inputs V_{11}, V_{22}, V_{31} are connected to grounded (A_2 is not used in this case). With these progresses, the output becomes:

$$V_{out} = \frac{s^2C_1C_2(-V_{32}) + sC_1g_{m2}V_{in} + g_{m1}g_{m2}(-V_{12})}{s^2C_1C_2 + sC_1g_{m2} + g_{m1}g_{m2}} \tag{19}$$

Combining (12), (14), (19), the transfer function can be expressed as:

$$V_{out-BP-I} = \frac{sC_1g_{m2}V_{in}}{s^2C_1C_2(1 + g_{m3}R_3) + sC_1g_{m2} + g_{m1}g_{m2}(1 + g_{m3}R_1)} \tag{20}$$

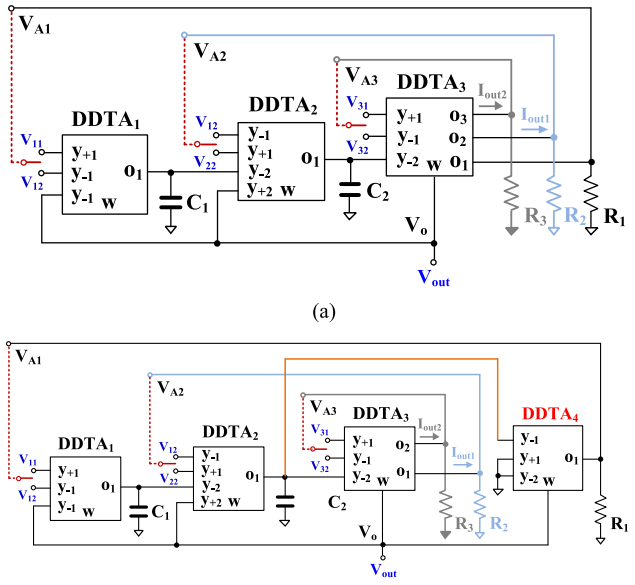

FIGURE 6. Proposed shadow filter using MIMO-DDTAs, (a) using minimum active device, (b) obtaining independent control.

Letting $R_1 = R_3 = R(A_1 = A_3 = A)$, the parameters ω_o and Q of the low-pass, high-pass, and band-pass filters in case I can be expressed by:

$$\omega_o = \sqrt{\frac{g_{m1}g_{m2}}{C_1C_2}} \tag{21}$$

$$Q = (1 + g_{m3}R)\sqrt{\frac{C_2g_{m1}}{C_1g_{m2}}} \tag{22}$$

The parameter Q can be controlled using amplifier A by R or g_{m3} without affecting parameter ω_o.

In case I, when the amplifier A_2 is used and if R_2 is removed, the circuit can work in transimpedance mode (TIM). The I_{out1} will be used as the output current. From (16), (18), (20), the TIM of the low-pass ($I_{out-LP-I}$), high-pass ($I_{out-HP-I}$), and band-pass ($I_{out-BP-I}$) filters is given respectively by:

$$\left.\begin{aligned} I_{out-LP-I} &= g_{m3}V_{out-LP} \\ I_{out-HP-I} &= g_{m3}V_{out-HP} \\ I_{out-BP-I} &= g_{m3}V_{out-BP} \end{aligned}\right\} \tag{23}$$

In this case, the resistor R is more suitable for adjusting the parameter Q.

Case II

The input signal V_{in} is applied to V_{12}, the input V_{11} is connected to V_{A1} (A_1), the input V_{21} is connected to V_{A2} (A_2), and the inputs V_{22}, V_{31}, V_{33} are connected to ground (A_3 is not used in this case). With these assumptions, the output becomes:

$$V_o = \frac{sC_1g_{m2}V_{21} + g_{m1}g_{m2}(V_{11} - V_{in})}{s^2C_1C_2 + sC_1g_{m2} + g_{m1}g_{m2}} \tag{24}$$

Combining (12), (13), (24), the transfer function can be expressed as

$$V_{out-LP-II} = \frac{-g_{m1}g_{m2}V_{in}}{s^2C_1C_2 + sC_1g_{m2}(1 - g_{m3}R_2) + g_{m1}g_{m2}(1 - g_{m3}R_1)} \tag{25}$$

If A_3 is used and node V_{A3} becomes the output, the passband gain of the low-pass filter can be controlled by $g_{m3}R_3$.

The input signal V_{in} is applied to V_{31}, the input V_{11} is connected to V_{A1} (A_1), the input V_{21} is connected to V_{A2} (A_2), and the inputs V_{12}, V_{22}, V_{32} are connected to ground (A_3 is not used in this case). With these assumptions, the output becomes:

$$V_o = \frac{s^2C_1C_2V_{in} + sC_1g_{m2}V_{21} + g_{m1}g_{m2}V_{11}}{s^2C_1C_2 + sC_1g_{m2} + g_{m1}g_{m2}} \tag{26}$$

Combining (12), (13), (26), the transfer function can be expressed as:

$$V_{out-HP-II} = \frac{s^2C_1C_2V_{in}}{s^2C_1C_2 + sC_1g_{m2}(1 - g_{m3}R_2) + g_{m1}g_{m2}(1 - g_{m3}R_1)} \tag{27}$$

If A_3 is used and node V_{A3} becomes the output, the passband gain of high-pass filter can be controlled by $g_{m3}R_3$.

The input signal V_{in} is applied to V_{22}, the input V_{11} is connected to V_{A1} (A_1), the input V_{21} is connected to V_{A2} (A_2), and the inputs V_{12}, V_{31}, V_{32} are connected to ground (A_3 is not used in this case). With these assumptions, the output becomes:

$$V_o = \frac{sC_1g_{m2}(V_{21} - V_{in}) + g_{m1}g_{m2}V_{11}}{s^2C_1C_2 + sC_1g_{m2} + g_{m1}g_{m2}} \tag{28}$$

Combining (12), (13), (28), the transfer function can be expressed as:

$$V_{out-BP-II} = \frac{-sC_1g_{m2}V_{in}}{s^2C_1C_2 + sC_1g_{m2}(1 - g_{m3}R_2) + g_{m1}g_{m2}(1 - g_{m3}R_1)} \tag{29}$$

If A_3 is used and node V_{A3} becomes the output, the passband gain of band-pass filter can be controlled by $g_{m3}R_3$.

The input signal V_{in} is applied to V_{12} and V_{32} together, the input V_{11} is connected to V_{A1} (A_1), the input V_{21} is connected to V_{A2} (A_2), and the inputs V_{22}, V_{31} are connected to ground

$$V_o = \frac{s^2C_1C_2(V_{31} - V_{32}) + sC_1g_{m2}(V_{21} - V_{22}) + g_{m1}g_{m2}(V_{11} - V_{12})}{s^2C_1C_2 + sC_1g_{m2} + g_{m1}g_{m2}} \tag{11}$$

(A_3 is not used in this case). With these assumptions, the output becomes:

$$V_o = \frac{s^2C_1C_2\,(-V_{in}) + sC_1g_{m2}\,(V_{21}) + g_{m1}g_{m2}\,(V_{11} - V_{in})}{s^2C_1C_2 + sC_1g_{m2} + g_{m1}g_{m2}} \tag{30}$$

Combining (12), (13), (30), the transfer function can be expressed as:

$$V_{out-BS-II} = \frac{-\left(s^2C_1C_2 + g_{m1}g_{m2}\right)V_{in}}{s^2C_1C_2 + sC_1g_{m2}\,(1 - g_{m3}R_2) + g_{m1}g_{m2}\,(1 - g_{m3}R_1)} \tag{31}$$

If A_3 is used and node V_{A3} becomes the output, the passband gain of the band-stop filter can be controlled by $g_{m3}R_3$.

The parameters ω_o and Q can be expressed by:

$$\omega_o = \sqrt{\frac{g_{m1}g_{m2}\,(1 - g_{m3}R_1)}{C_1C_2}} \tag{32}$$

$$Q = \frac{\sqrt{1 - g_{m3}R_1}}{1 - g_{m3}R_2}\sqrt{\frac{g_{m1}C_2}{g_{m2}C_1}} \tag{33}$$

The parameter ω_o can be controlled by A_1 using $g_{m3}R_1$ and the parameter Q can be controlled by A_2 using $g_{m3}R_2$ without affecting the parameter ω_o. Controlling the frequency ω_o by A_1 will affect the quality factor Q. Therefore, in such case, the amplifier A_2 should be used to control Q.

In case II, when the amplifier A_3 is used and if R_3 is removed, the circuit can work in transimpedance mode (TIM). The I_{out2} will be treated as output current of TIM. From (25), (27), (29), (30), the TIM of low-pass ($I_{out-LP-II}$), high-pass ($I_{out-HP-II}$), band-pass ($I_{out-BP-II}$), and band-stop ($I_{out-BS-II}$) filters can be expressed respectively by:

$$\left.\begin{aligned} I_{out-LP-II} &= g_{m3}V_{out-LP} \\ I_{out-HP-II} &= g_{m3}V_{out-HP} \\ I_{out-BP-II} &= g_{m3}V_{out-BP} \\ I_{out-BS-II} &= g_{m3}V_{out-BS} \end{aligned}\right\} \tag{34}$$

In this case, the resistor R is more suitable for adjusting the parameter Q.

It should be noted for Case II that the parameters ω_o and Q are controlled by R_1 and R_2. Fig. 6 (b) shows the modified shadow filter to obtain electronic and independent control of the parameters ω_o and Q by adding additional DDTA$_4$.The parameters ω_o and Q of Fig. 6 (b) can be expressed by:

$$\omega_o = \sqrt{\frac{g_{m1}g_{m2}\,(1 - g_{m4}R_1)}{C_1C_2}} \tag{35}$$

$$Q = \frac{\sqrt{1 - g_{m4}R_1}}{1 - g_{m3}R_2}\sqrt{\frac{g_{m1}C_2}{g_{m2}C_1}} \tag{36}$$

The parameter ω_o can be controlled by A_1 using g_{m4} and parameter Q can be controlled by A_2 using g_{m3} without affecting the parameter ω_o. Therefore, the parameter ω_o and Q of the shadow filter in Fig. 6 (b) can be electronically and independently controlled.

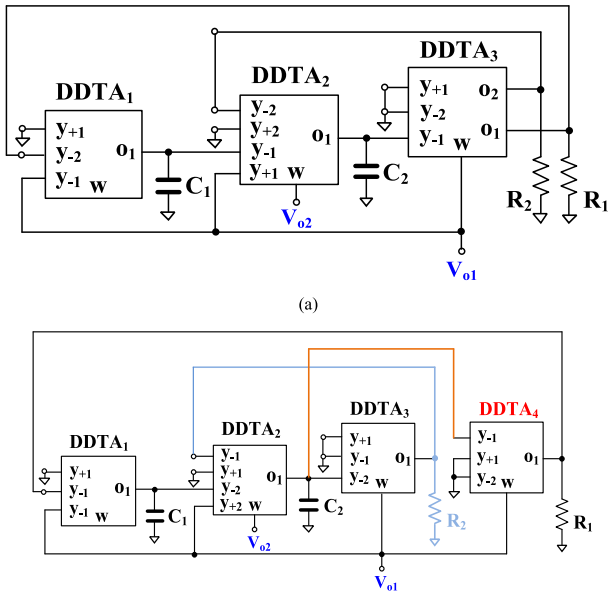

FIGURE 7. Modified shadow oscillator, (a) with minimum DDTAs, (b) with independent and electronic tuning ability.

C. PROPOSED SHADOW OSCILLATOR

The proposed shadow filter was modified to a shadow oscillator as shown in Fig. 7. This oscillator uses the amplifiers to control the condition of oscillation and the frequency of oscillation. From Fig. 7 (a), the outputs V_{A1} and V_{A2} of the amplifiers A_1 and A_2, are connected respectively to the inputs V_{12} and V_{21} of the shadow filter while the amplifier A_3 is not used. The input terminals V_{11}, V_{22}, V_{31}, and V_{32} that are not used should be connected to ground. From Fig. 7 (a), the characteristic equation of the shadow oscillator can be expressed by:

$$s^2C_1C_2 + sC_1g_{m2}\,(1 - g_{m3}R_2) + g_{m1}g_{m2}\,(1 + g_{m3}R_1) = 0 \tag{37}$$

The condition of oscillation is:

$$1 - g_{m3}R_2 = 0 \tag{38}$$

The frequency of oscillation is:

$$\omega_o = \sqrt{\frac{g_{m1}g_{m2}}{C_1C_2}\,(1 + g_{m3}R_1)} \tag{39}$$

The condition of oscillation can be controlled by the amplifier A_2 using $g_{m3}R_2$ and the frequency of oscillation can be controlled by the amplifier A_1 using $g_{m3}R_1$. Thus, the condition of oscillation can be controlled by adjusting R_2 while the frequency of oscillation can be controlled by adjusting R_1, therefore, the proposed shadow oscillator provides independent control of the condition and frequency of oscillation.

Consider nodes V_{o1} and V_{o2} in Fig. 7 (a), the transfer function can be expressed by:

$$\frac{V_{o1}}{V_{o2}} = -\frac{g_{m2}}{sC_2} \tag{40}$$

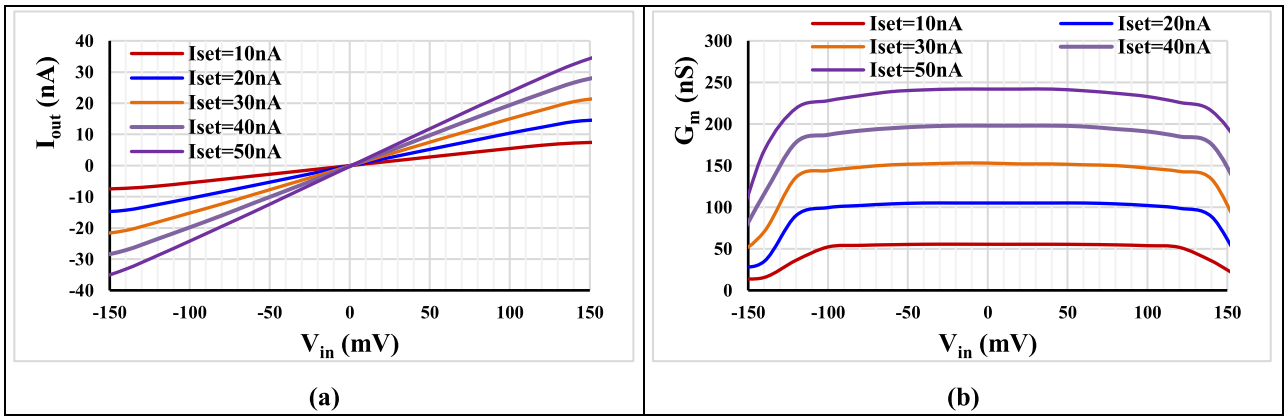

FIGURE 8. The MI-OTA output current (a) and the transconductance (b) versus the input voltage with various I_{set}.

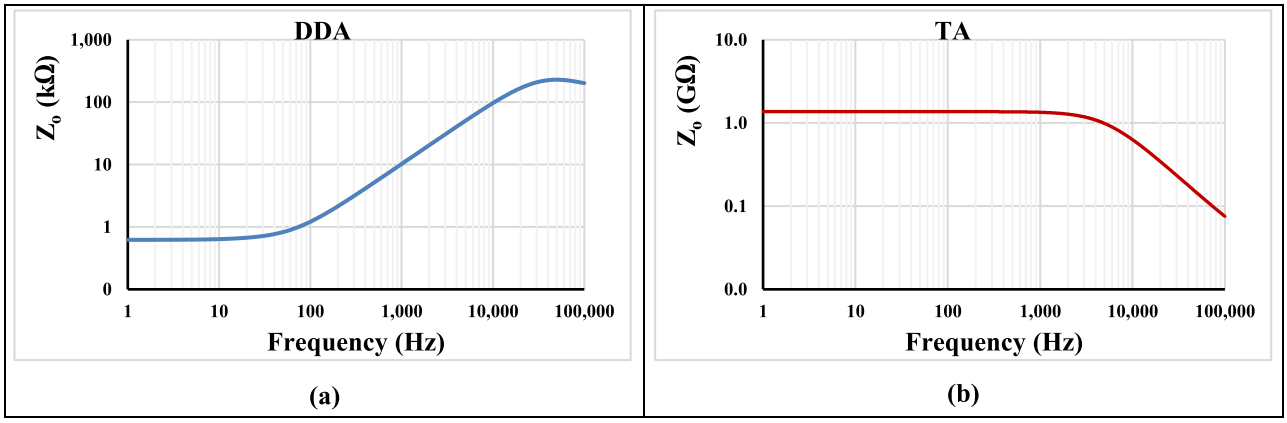

FIGURE 9. The output impedances of the DDA (a) and TA (b).

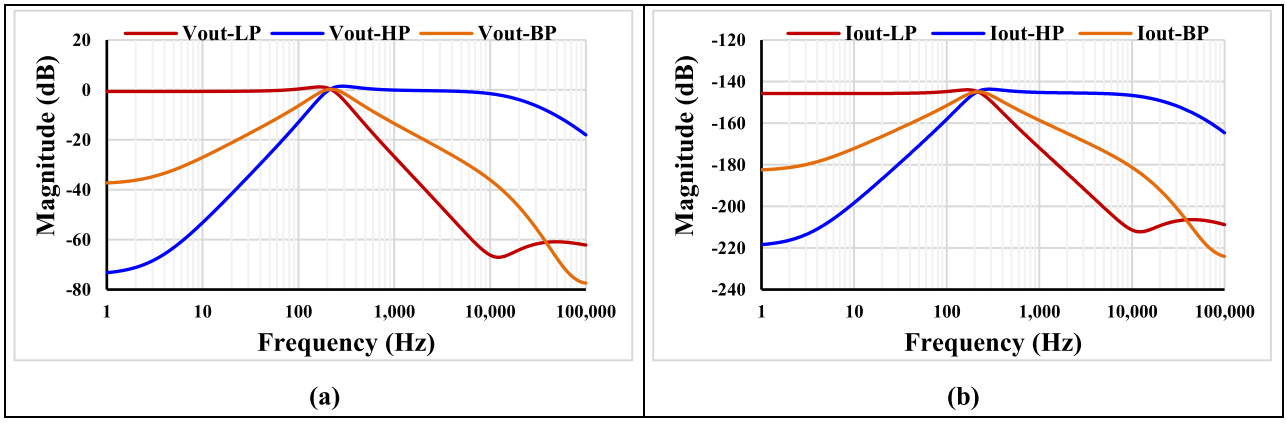

FIGURE 10. The frequency characteristic of the output voltages and currents of the shadow filter case I.

The phase difference between nodes V_{o1} and V_{o2} is 90°, i.e. these signals are in quadrature, while the magnitude is $|g_{m2}/C_2|$.

The shadow oscillator in Fig. 7 (a) can be modified to obtain electronic and independent control, by adding additional DDTA as shown Fig. 7 (b). The characteristic equation is:

$$s^2C_1C_2 + sC_1g_{m2}(1 - g_{m3}R_2) + g_{m1}g_{m2}(1 + g_{m4}R_1) = 0 \quad (41)$$

The condition of oscillation is:

$$1 - g_{m3}R_2 = 0 \quad (42)$$

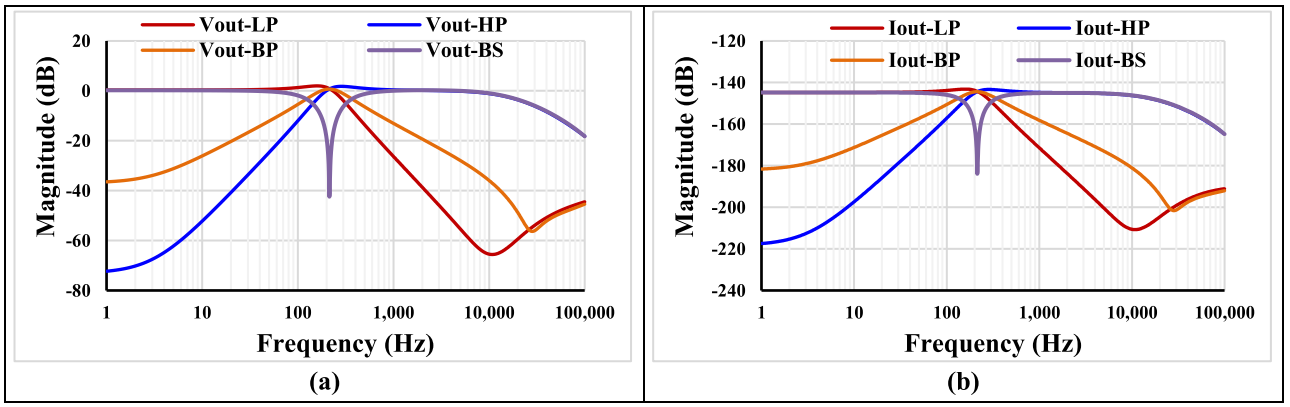

FIGURE 11. The frequency characteristic of the output voltages and currents of the shadow filter case II.

The frequency of oscillation can be given by:

$$\omega_o = \sqrt{\frac{g_{m1}g_{m2}}{C_1C_2}\left(1 + g_{m4}R_1\right)} \tag{43}$$

It is evident from (42) and (43) that the condition of oscillation can be controlled electronically by g_{m3} while the frequency of oscillation can be controlled electronically by g_{m4}. Hence the shadow oscillator in Fig. 7 (b) provides independent and electronic control of the condition of oscillation and the frequency of oscillation. The output nodes are V_{o1} and V_{o2}.

D. NON-IDEALITIES ANALYSIS

Considering the non-idealities of DDTA, (1) can be rewritten as:

$$\left.\begin{aligned} V_w = \beta_{+kj}V_{y+kj} + \beta_{+kj}V_{y+kj} - \beta_{-ki}V_{y-ki} - \beta_{-kj}V_{y-kj} \\ I_{o1} = I_{o2} = g_{mnk}V_w \end{aligned}\right\} \tag{44}$$

where $\beta_{+kj} = 1-\varepsilon_{+kj}$ and $\varepsilon_{+kj}\left(\left|\varepsilon_{+kj}\right| \ll 1\right)$ denotes the voltage tracking error from V_{y+j}-terminal to V_w-terminal, $\beta_{-kj} = 1-\varepsilon_{-kj}$ and $\varepsilon_{-kj}\left(\left|\varepsilon_{-kj}\right| \ll 1\right)$ denotes the voltage tracking error from V_{y-j}-terminal to V_w-terminal of the $k-$ th DDTA and the $j-$th input terminal. The g_{mni} is the non-ideal transconductance gain of the DDTA. In the frequency range near the cut-off frequency, g_{mnk} can be approximated as:

$$g_{mnk}(s) \cong g_{mk}(1 - \mu_k s) \tag{45}$$

where $\mu_k = 1/\omega_{gmk}$, ω_{gk} denotes the first-order pole.

Using (45), the denominator of (11) becomes, as in (46), shown at the bottom of the next page.

Using (44), (16), (18), (20) in case-I can be rewritten as:

$$V_{out-LP-I} = \frac{g_{m1}g_{m2}\beta_{+11}\beta_{-31}V_{in}}{\left\{\begin{aligned} s^2C_1C_2\left(1 + g_{m3}R_3\beta_{-32}\right) + sC_1g_{mn2}\beta_{+21}\beta_{-31} \\ +g_{mn1}g_{mn2}\beta_{-11}\beta_{-31}\left(1 + g_{m3}R_1\beta_{-12}\beta_{-31}\right)\end{aligned}\right\}} \tag{47}$$

TABLE 1. Transistor aspect ratio of the DDTA.

DDA	W/L (μm/μm)
M_{1A}, M_{2A}, M_{1B}, M_{2B} M_{14}, M_{15}	16/3
M_3-M_8, M_{11}-M_{12}, M_B	8/3
M_9, M_{10}	4/3
M_{16}	6×16/3
M_{13}	6×8/3
M_R	4/5
MIM capacitor: C_B= 0.5 pF, C_c= 6 pF	
TA	**W/L (μm/μm)**
M_1, M_2	4×1.2/1.2
M_{15}, M_{16}	2×1.2/1.2
M_{3D}, M_{4D}, M_{7D}, M_{8D}, M_{9D}	4/1.2
M_{3S}, M_{4S}, M_{7S}, M_{8S}, M_{9S}	4/0.2
M_{5D}, M_{6D}	1.2/1.2
M_{5S}, M_{6S}	1.2/0.2
M_{10D}, M_{11D}, M_{12D}	8/1.2
M_{10S}, M_{11S}, M_{12S}	8/0.2
M_{13D}, M_{14D}	10/1.2
M_{13S}, M_{14S}	10/0.2
M_{17D}	20/1.2
M_{17S}	20/0.2

$$V_{out-HP-I} = \frac{s^2C_1C_2\beta_{+31}V_{31}}{\left\{\begin{aligned} s^2C_1C_2\left(1 + g_{m3}R_3\beta_{-32}\right) + sC_1g_{mn2}\beta_{+21}\beta_{-31} \\ +g_{mn1}g_{mn2}\beta_{-11}\beta_{-31}\left(1 + g_{m3}R_1\beta_{-12}\beta_{-31}\right)\end{aligned}\right\}} \tag{48}$$

$$V_{out-BP-I} = \frac{sC_1g_{m2}\beta_{-21}\beta_{-31}V_{in}}{\left\{\begin{aligned} s^2C_1C_2\left(1 + g_{m3}R_3\beta_{-32}\right) + sC_1g_{mn2}\beta_{+21}\beta_{-31} \\ +g_{mn1}g_{mn2}\beta_{-11}\beta_{-31}\left(1 + g_{m3}R_1\beta_{-12}\beta_{-31}\right)\end{aligned}\right\}} \tag{49}$$

The parameters ω_o and Q in (21), (22) can be rewritten as:

$$\omega_o = \sqrt{\frac{g_{mn1}g_{mn2}\beta_{-11}\beta_{-31}\left(1 + g_{m3}R_1\beta_{-12}\beta_{-31}\right)}{C_1C_2\left(1 + g_{m3}R_3\beta_{-32}\right)}} \tag{50}$$

$$Q = \sqrt{\left(1 + g_{m3}R_1\beta_{-12}\beta_{-31}\right)\left(1 + g_{m3}R_3\beta_{-32}\right)} \times \sqrt{\frac{g_{mn1}C_2\beta_{-11}\beta_{-31}}{g_{mn2}C_1\beta_{+21}\beta_{-31}}} \tag{51}$$

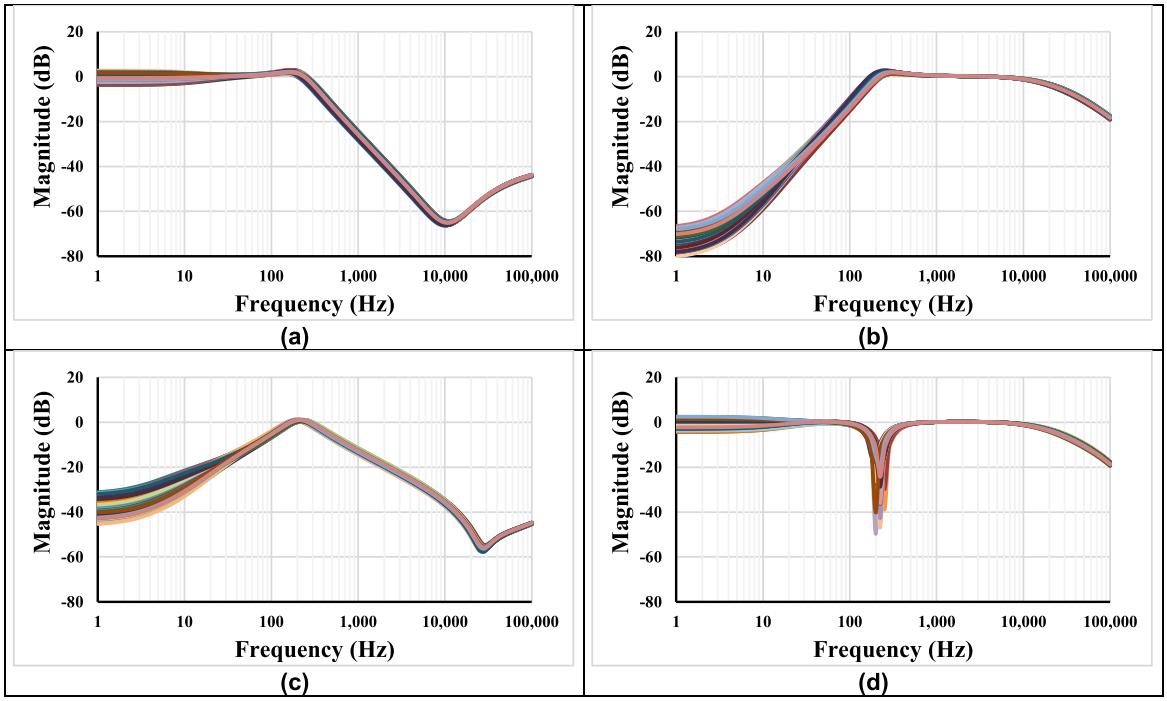

FIGURE 12. The frequency characteristic of the output voltages with MC analysis for LP (a), HP (b), BP (c) and BS (d).

Using (44), (25), (27), (29), (31) in case-II can be rewritten as

$$V_{out-LP-II} = \frac{-g_{m1}g_{m2}\beta_{-12}\beta_{-31}V_{in}}{\left\{\begin{array}{l} s^2C_1C_2 + sC_1g_{mn2}\beta_{+21}\beta_{-31}\left(1-g_{m3}R_2\beta_{-21}\beta_{-31}\right) \\ +g_{mn1}g_{mn2}\beta_{-11}\beta_{-31}\left(1-g_{m3}R_1\beta_{+11}\beta_{-31}\right) \end{array}\right\}} \quad (52)$$

$$V_{out-HP-II} = \frac{s^2C_1C_2\beta_{+31}V_{in}}{\left\{\begin{array}{l} s^2C_1C_2 + sC_1g_{mn2}\beta_{+21}\beta_{-31}\left(1-g_{m3}R_2\beta_{-21}\beta_{-31}\right) \\ +g_{mn1}g_{mn2}\beta_{-11}\beta_{-31}\left(1-g_{m3}R_1\beta_{+11}\beta_{-31}\right) \end{array}\right\}} \quad (53)$$

$$V_{out-BP-II} = \frac{-sC_1g_{m2}\beta_{+11}\beta_{-31}V_{in}}{\left\{\begin{array}{l} s^2C_1C_2 + sC_1g_{mn2}\beta_{+21}\beta_{-31}\left(1-g_{m3}R_2\beta_{-21}\beta_{-31}\right) \\ +g_{mn1}g_{mn2}\beta_{-11}\beta_{-31}\left(1-g_{m3}R_1\beta_{+11}\beta_{-31}\right) \end{array}\right\}} \quad (54)$$

$$V_{out-BS-II} = \frac{-\left(s^2C_1C_2\beta_{-32} + g_{mn1}g_{mn2}\beta_{-12}\beta_{-31}\right)V_{in}}{\left\{\begin{array}{l} s^2C_1C_2 + sC_1g_{mn2}\beta_{+21}\beta_{-31}\left(1-g_{m3}R_2\beta_{-21}\beta_{-31}\right) \\ +g_{mn1}g_{mn2}\beta_{-11}\beta_{-31}\left(1-g_{m3}R_1\beta_{+11}\beta_{-31}\right) \end{array}\right\}} \quad (55)$$

The parameters ω_o and Q in (21), (22) can be rewritten as:

$$\omega_o = \sqrt{\frac{g_{mn1}g_{mn2}\beta_{-11}\beta_{-31}\left(1-g_{m3}R_1\beta_{+11}\beta_{-31}\right)}{C_1C_2}} \quad (56)$$

$$Q = \frac{\sqrt{\left(1-g_{m3}R_1\beta_{+11}\beta_{-31}\right)}}{\left(1-g_{m3}R_2\beta_{-21}\beta_{-31}\right)\beta_{+21}\beta_{-31}}\sqrt{\frac{g_{mn1}C_2\beta_{-11}\beta_{-31}}{g_{mn2}C_1}} \quad (57)$$

Considering the non-ideal shadow oscillator in Fig. 7(a), the characteristic equation can be expressed by:

$$s^2C_1C_2 + sC_1g_{mn2}\beta_{+21}\beta_{-31}\left(1-g_{m3}R_2\beta_{-21}\beta_{-31}\right) + g_{mn1}g_{mn2}\beta_{-11}\beta_{-31}\left(1+g_{m3}R_1\beta_{-12}\beta_{-31}\right) = 0 \quad (58)$$

The condition of oscillation is rewritten as:

$$1 - g_{m3}R_2\beta_{-21}\beta_{-31} = 0 \quad (59)$$

and the frequency of oscillation is rewritten as:

$$\omega_o = \sqrt{\frac{g_{mn1}g_{mn2}\beta_{-11}\beta_{-31}\left(1+g_{m3}R_1\beta_{+11}\beta_{-31}\right)}{C_1C_2}} \quad (60)$$

III. SIMULATION RESULTS

The DDTA circuit, the shadow filter and the oscillator were designed in Cadence program using CMOS technology 0.18 μm from TSMC. The DDTA voltage supply was 0.5 V.

$$V_o = \frac{\left\{\begin{array}{l} s^2C_1C_2\left(V_{31}\beta_{+31} - V_{32}\beta_{-32}\right) + sC_1g_{m2}\left(V_{21}\beta_{-21}\beta_{-31} - V_{22}\beta_{+11}\beta_{-31}\right) \\ +g_{m1}g_{m2}\left(V_{11}\beta_{+11}\beta_{-31} - V_{12}\beta_{-12}\beta_{-31}\right) \end{array}\right\}}{s^2C_1C_2 + sC_1g_{mn2}\beta_{+21}\beta_{-31} + g_{mn1}g_{mn2}\beta_{-11}\beta_{-31}} \quad (46)$$

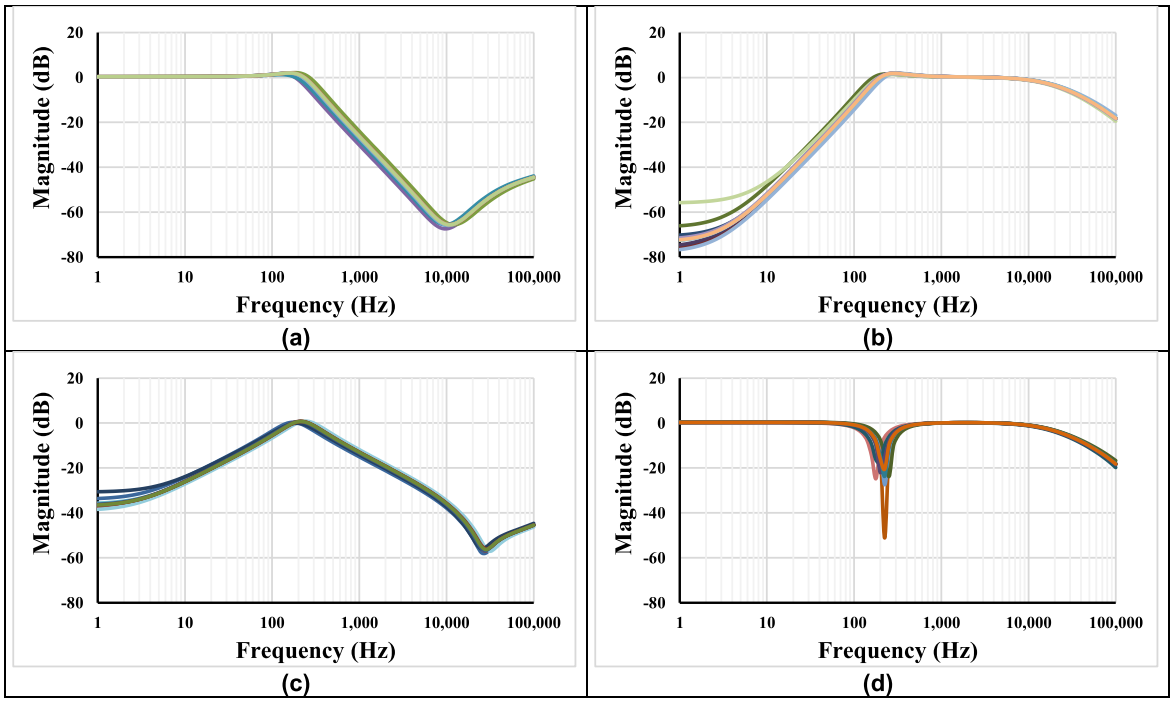

FIGURE 13. The frequency characteristic of the output voltages with PVT analysis for LP (a), HP (b), BP (c) and BS (d).

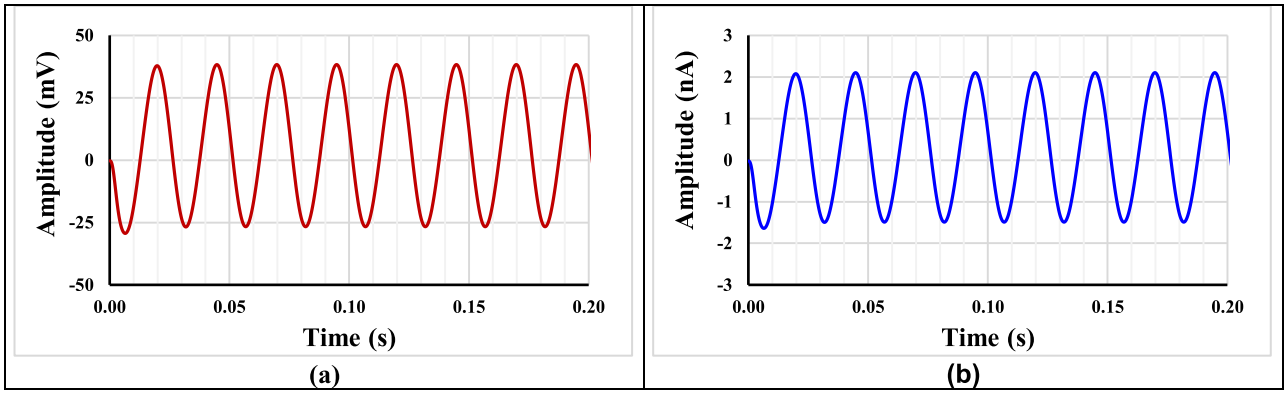

FIGURE 14. The transient response of the LP filter case II, voltage output (a) and current output (b).

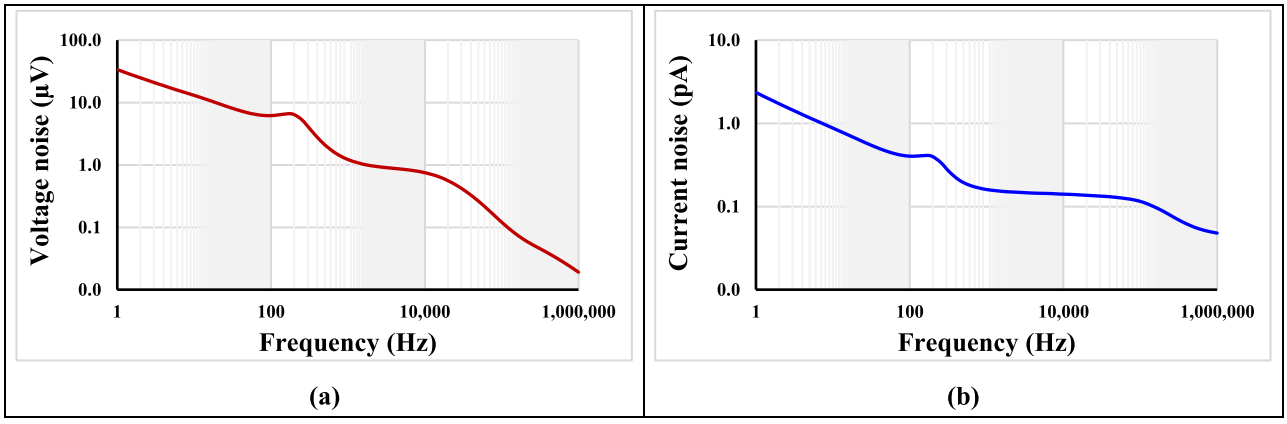

FIGURE 15. The output equivalent noise the LP filter case II, voltage output (a) and current output (b).

The DDA bias current was 40 nA and the nominal setting current was 10 nA for the TA. The power consumption of the DDTA was 218.2 nW (DDA = 203nW, two outputs TA = 15.25 nW). The transistor's aspect ratio of the DDTA

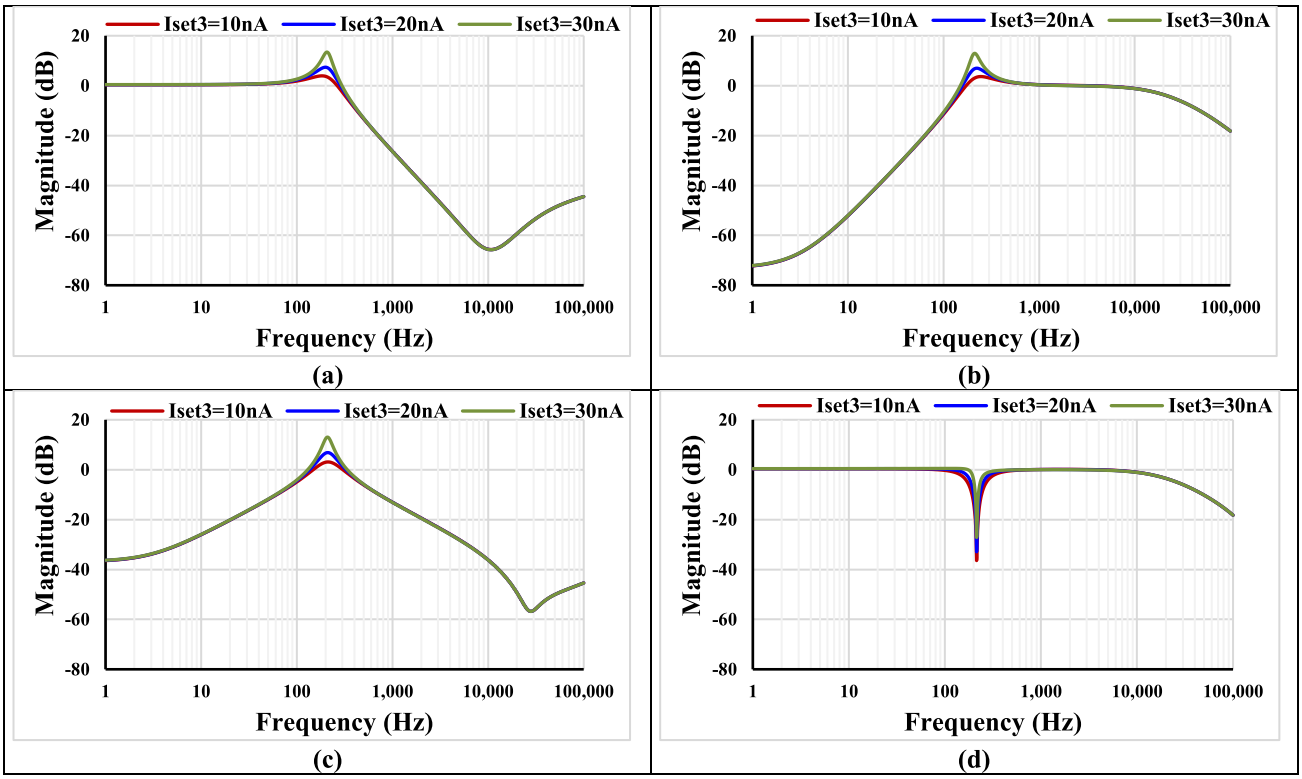

FIGURE 16. Tuning of Q parameter for LP (a), HP (b), BP (c) and BS (d).

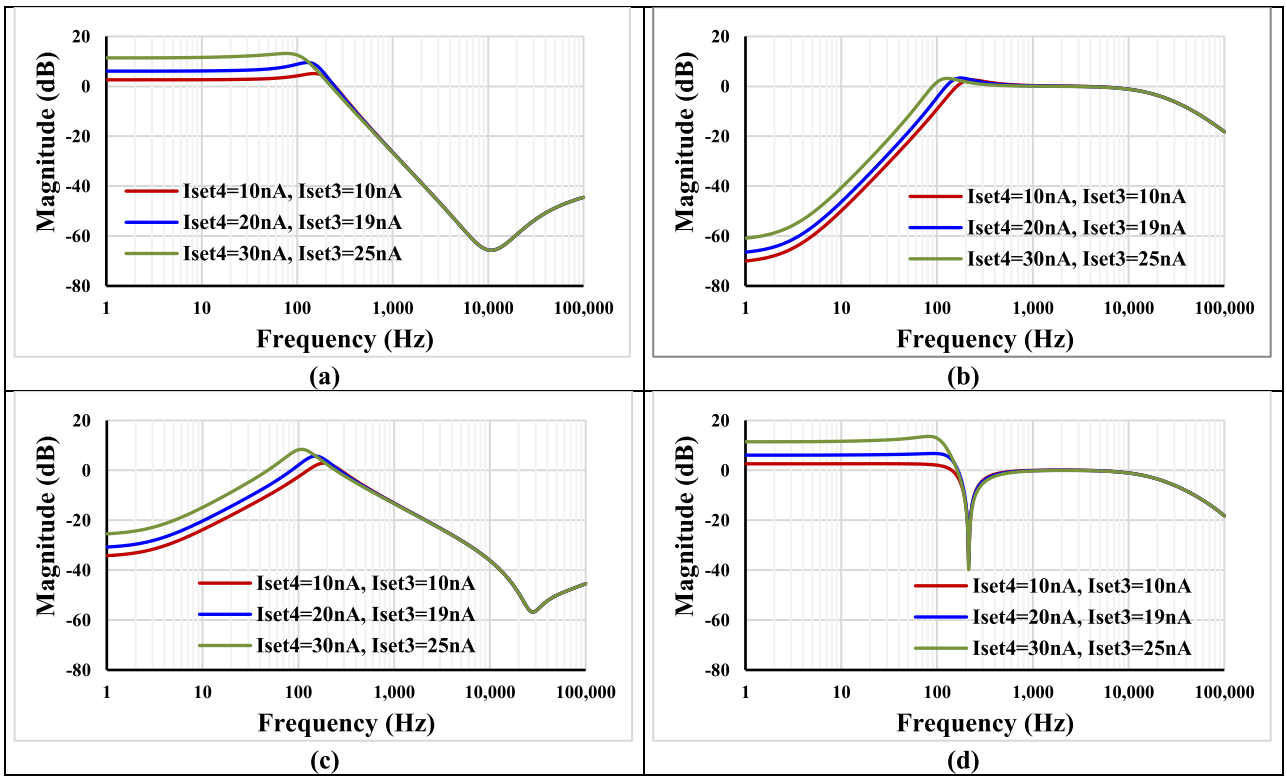

FIGURE 17. Tuning of ω_o parameter for LP (a), HP (b), BP (c) and BS (d).

is shown in Table 1. The output current and the transconductance versus input voltage of the TA is shown in Fig. 8. As it is evident, the TA enjoys high linearity in range of ±100mV. The output impedance of the DDA (connected as DDCC) and

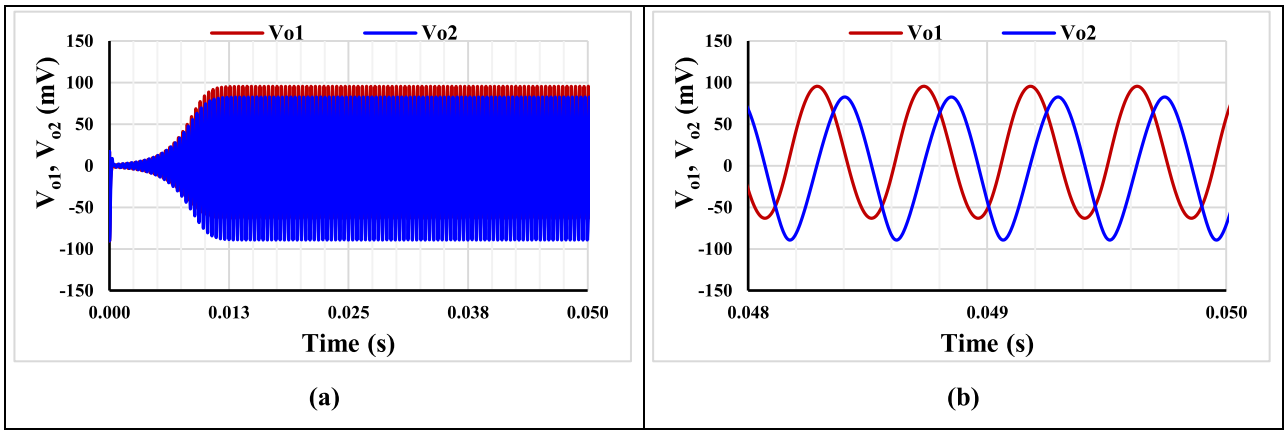

FIGURE 18. The running oscillation (a) and the steady state (b) of the shadow oscillator.

TABLE 2. Properties comparison of this work with those of shadow filters.

Factor	Proposed	[23]	[28]	[30]	[40]	[42]	[43]
Number of active devices	4DDTA	3-6 CFOA	3 OFCC	2 CDCTA	2 VDGA	3 VDDDA	4OTA
Realization	CMOS structure	commercial IC	CMOS structure & commercial IC	CMOS structure & commercial IC	CMOS structure	CMOS structure & commercial IC	CMOS structure
Number capacitors	2C, 3R	2 C, 4-9 R	2 R, 2C	2C	2C	1 R, 2C	2-C
Type of filter	MISO	MISO	SIMO	SIMO	SIMO	SIMO	SIMO
Operation mode	VM/TIM	VM	CM	CM	VM	VM	VM
Number of offered responses	4	4	5	3	2	5	2
No need of buffer circuit at input or output	Yes	No	Yes	No	No	No	No
All grounded capacitors	Yes	No	Yes	Yes	Yes	Yes	Yes
Independent control of ω_o and Q	Yes	Yes	Yes	Yes	Yes	Yes	Yes
Electronic control	Yes	No	No	Yes	Yes	Yes	Yes
Offer modified into oscillator	Yes	No	No	No	No	No	No
Number phases of sinusoidal output	2	-	-	-	-	-	-
Simulated power supply (V)	0.5	-	±1.5	±1.25	±1	±0.9	±1.8
Simulated power dissipation (μW)	0.873	-	-	1500	-	-	-
Total harmonic distortion (%)	2@60mV_{pp}	-	-	<1@600μA	-	1@280mV_{pp}	<4%@60mV
Verification of result	Sim	Exp	Sim/Exp	Sim/Exp	Sim	Sim/Exp	Sim

Note: CFOA = current-feedback operational-amplifier, OFCC = operational floating current conveyor, CDCTA = differencing cascaded transconductance amplifier, VDGA = voltage differencing gain amplifier, VDDDA = voltage differencing differential difference amplifiers.

TA is shown in Fig. 9 the low frequency resistance of the DDA and OTA is 621 Ω and 1.36 GΩ, respectively.

For Fig. 6 (a), Fig. 10 and 11 show the AC characteristics of the output voltages and currents from case I and II, respectively, the values were: $C_1 = C_2 = 40$pF, $R_{1,2,3} = R_1 = R_2 = R_3 = 1$ MΩ, $I_{set1,2,3} = I_{set1} = I_{set2} = I_{set3} = 10$ nA ($g_m = 55.4$ nS). The simulated nature frequency was 214.3 Hz that is close to the calculated value 220 Hz. The calculated $Q = 1.03$.

The Monte Carlo, process and mismatch, analysis with 200 runs for the filter case II is shown in Fig. 12. Fig. 13 shows the process, voltage and temperature (PVT) corner analysis for process (fast-fast, fast-slow, slow-fast, slow-slow), voltage supply (V_{DD}±10%V_{DD}) and temperature (−20°C and 70°C). Both Figs. 12 and 13 confirm the stability of the proposed application.

The transient analysis for the current and voltage outputs of the LPF case II with input sine wave of 60mV peak-to-peak @ 40 Hz is shown on Fig. 14. The total harmonic distortion (THD) was around 2 %. The output equivalent noise for the LP filter for output voltage and current are shown in Fig. 15. The output integrated noise was 114.2μV and 7.54pA, respectively.

For Fig. 6 (b) is used to show the electronic tuning capability of the filter. Fig. 16 shows the tuning of the parameter Q without disturbing ω_o by controlling the A_2 via g_{m3}

(I_{set3} = 10 nA, 20 nA, 30 nA), with R_1 = 1 MΩ and R_2 =5 MΩ, and $I_{set1,2}$ = 10 nA. The calculated Q was 1.34, 2.05, 4.9.

The tuning capability of ω_o parameter is shown in Fig. 17 with $R_1 = R_2 = 5$ MΩ. The natural frequency was tuned in range 212 Hz – 253 Hz without affecting the parameter Q.

The shadow oscillator in Fig 7 was simulated for I_{set} = 10nA and R_1 = 1MΩ and R_2 = 19MΩ, the running oscillation and the steady state are shown in Fig. 18. The simulated frequency was 224Hz and the THD was around 2 %.

Finally, Table 2 provides the properties comparison of this work with other shadow filters. The voltage-mode MISO-type shadow filters in [23], current-mode SIMO-type shadow filters in [28] and [30], and voltage-mode SIMO-type shadow filters in [40], [42], and [43] have been used to compare. Compared with [23], the proposed filter has less amount of passive and active components, compared with [28], the proposed filter provides electronic tuning ability, and compared with [40] and [43], the proposed filter offers larger number of transfer functions. Compared with all shadow filters [23], [28], [30], [40], [42], [43], the proposed filter provides both VM and TIM filtering functions, uses lower supply voltage, and consumes less power.

IV. CONCLUSION

This paper presents new applications of multiple-input multiple-output DDTA using multiple-input bulk-driven MOS transistor technique. The multiple inputs of DDTA can be obtained using MIBD MOST technique without using additional MOS differential pair and results in minimum power dispassion. The multiple-output currents of the proposed DDTA are also available. To show the advantage of MIMO DDTA, it has been used to realize a multiple-input single-output (MISO) shadow filter. The proposed shadow filter with minimum number of active devices and independent electronic control of natural frequency and quality factor was achieved. Both voltage- and transimpedance-mode shadow filters can be obtained into single topology. It can be also shown that MISO shadow filter can be easily modified to work as a shadow oscillator with independent control of the frequency and the condition of oscillation. The simulation results confirm the performance of the proposed MIMO-DDTA and its applications.

REFERENCES

[1] A. Kumar and S. K. Paul, "DX-MOCCII based fully cascadable second order current-mode universal filter," *J. Circuits, Syst. Comput.*, vol. 27, no. 7, Jun. 2018, Art. no. 1850113, doi: 10.1142/S021812661850113X.

[2] L. Safari, G. Barile, G. Ferri, and V. Stornelli, "A new low-voltage low-power dual-mode VCII-based SIMO universal filter," *Electronics*, vol. 8, no. 7, p. 765, Jul. 2019, doi: 10.3390/electronics8070765.

[3] D. R. Bhaskar, A. Raj, and R. Senani, "Three new CFOA-based SIMO-type universal active filter configurations with unrivalled features," *AEU Int. J. Electron. Commun.*, vol. 153, Aug. 2022, Art. no. 154285, doi: 10.1016/j.aeue.2022.154285.

[4] H.-P. Chen, S.-F. Wang, Y. Ku, A.-C. Yeh, and Y.-H. Chen, "Design of second-order multifunction filter IC based on current feedback amplifiers with independent voltage gain control," *IEEE Access*, vol. 10, pp. 63301–63313, 2022, doi: 10.1109/ACCESS.2022.3183226.

[5] M. Kumngern, B. Knobnob, and K. Dejhan, "Electronically tunable high-input impedance voltage-mode universal biquadratic filter based on simple CMOS OTAs," *AEU Int. J. Electron. Commun.*, vol. 64, no. 10, pp. 934–939, Oct. 2010, doi: 10.1016/j.aeue.2009.07.015.

[6] C.-N. Lee, "Independently tunable plus-type DDCC-based voltage-mode universal biquad filter with MISO and SIMO types," *Microelectron. J.*, vol. 67, pp. 71–81, Sep. 2017, doi: 10.1016/j.mejo.2017.07.006.

[7] W. Jaikla, F. Khateb, T. Kulej, and K. Pitaksuttayaprot, "Universal filter based on compact CMOS structure of VDDDA," *Sensors*, vol. 21, no. 5, p. 1683, Mar. 2021, doi: 10.3390/s21051683.

[8] W. Jaikla, F. Khateb, M. Kumngern, T. Kulej, R. K. Ranjan, and P. Suwanjan, "0.5 V fully differential universal filter based on multiple input OTAs," *IEEE Access*, vol. 8, pp. 187832–187839, 2020, doi: 10.1109/ACCESS.2020.3030239.

[9] M. Faseehuddin, N. Herencsar, S. Shireen, W. Tangsrirat, and S. H. M. Ali, "Voltage differencing buffered amplifier-based novel truly mixed-mode biquadratic universal filter with versatile input/output features," *Appl. Sci.*, vol. 12, no. 3, p. 1229, Jan. 2022, doi: 10.3390/app12031229.

[10] S.-F. Wang, H.-P. Chen, Y. Ku, and C.-M. Yang, "Independently tunable voltage-mode OTA-C biquadratic filter with five inputs and three outputs and its fully-uncoupled quadrature sinusoidal oscillator application," *AEU Int. J. Electron. Commun.*, vol. 110, Oct. 2019, Art. no. 152822, doi: 10.1016/j.aeue.2019.152822.

[11] S.-F. Wang, H.-P. Chen, Y. Ku, and Y.-C. Lin, "Versatile tunable voltage-mode biquadratic filter and its application in quadrature oscillator," *Sensors*, vol. 19, no. 10, p. 2349, May 2019, doi: 10.3390/s19102349.

[12] D. Agrawal and S. Maheshwari, "High-performance electronically tunable analog filter using a single EX-CCCII," *Circuits, Syst., Signal Process.*, vol. 40, no. 3, pp. 1127–1151, Mar. 2021, doi: 10.1007/s00034-020-01530-7.

[13] W. Chiu, S. I. Liu, H. W. Tsao, and J. J. Chen, "CMOS differential difference current conveyors and their applications," *IEE Proc. Circuits, Devices Syst.*, vol. 143, no. 2, pp. 91–96, Apr. 1996, doi: 10.1049/ip-cds:19960223.

[14] A. A. El-Adawy, A. M. Soliman, and H. O. Elwan, "A novel fully differential current conveyor and applications for analog VLSI," *IEEE Trans. Circuits Syst. II, Analog Digit. Signal Process.*, vol. 47, no. 4, pp. 306–313, Apr. 2000, doi: 10.1109/82.839666.

[15] C. Wang, H. Liu, and Y. Zhao, "A new current-mode current-controlled universal filter based on CCCII(±)," *Circuits, Syst. Signal Process.*, vol. 27, no. 5, pp. 673–682, Oct. 2008, doi: 10.1007/s00034-008-9050-y.

[16] K. Garradhi, N. Hassen, T. Ettaghzouti, and K. Besbes, "Realization of current-mode biquadratic filter employing multiple output OTAs and MO-CCII," *AEU Int. J. Electron. Commun.*, vol. 83, pp. 168–179, Jan. 2018, doi: 10.1016/j.aeue.2017.08.027.

[17] E. Rodriguez-Villegas, A. Yufera, and A. Rueda, "A 1.25-V micropower Gm-C filter based on FGMOS transistors operating in weak inversion," *IEEE J. Solid-State Circuits*, vol. 39, no. 1, pp. 100–111, Jan. 2004, doi: 10.1109/JSSC.2003.820848.

[18] O. Omeni, E. Rodriguez-Villegas, and C. Toumazou, "A micropower CMOS continuous-time filter with on-chip automatic tuning," *IEEE Trans. Circuits Syst. I, Reg. Papers*, vol. 52, no. 4, pp. 695–705, Apr. 2005, doi: 10.1109/TCSI.2005.844112.

[19] I.-Y. Lee, D. Im, J. Ko, and S.-G. Lee, "A 50–450 MHz tunable RF biquad filter based on a wideband source follower with > 26 dBm IIP_3, +12 dBm P_{1dB}, and 15 dB noise figure," *IEEE J. Solid-State Circuits*, vol. 50, no. 10, pp. 2294–2305, Oct. 2015, doi: 10.1109/JSSC.2015.2468722.

[20] Y. Lakys and A. Fabre, "Shadow filters–new family of second-order filters," *Electron. Lett.*, vol. 46, no. 4, pp. 276–277, 2010, doi: 10.1049/el.2010.3249.

[21] Y. Lakys and A. Fabre, "Shadow filters generalisation to *n*th-class," *Electron. Lett.*, vol. 46, no. 14, pp. 985–986, 2010, doi: 10.1049/el.2010.0452.

[22] V. Biolkova and D. Biolek, "Shadow filters for orthogonal modification of characteristic frequency and bandwidth," *Electron. Lett.*, vol. 46, no. 12, pp. 830–831, 2010, doi: 10.1049/el.2010.0717.

[23] M. T. Abuelma'atti and N. R. Almutairi, "New current-feedback operational-amplifier based shadow filters," *Anal. Integr. Circuits Signal Process.*, vol. 86, no. 3, pp. 471–480, Mar. 2016, doi: 10.1007/s10470-016-0691-7.

[24] N. Pandey, R. Pandey, R. Choudhary, A. Sayal, and M. Tripathi, "Realization of CDTA based frequency agile filter," in *Proc. IEEE Int. Conf. Signal Process., Comput. Control (ISPCC)*, Sep. 2013, pp. 1–6, doi: 10.1109/ISPCC.2013.6663403.

[25] E. Alaybeyoğlu, A. Güney, M. Altun, and H. Kuntman, "Design of positive feedback driven current-mode amplifiers Z-copy CDBA and CDTA, and filter applications," *Anal. Integr. Circuits Signal Process.*, vol. 81, no. 1, pp. 109–120, Oct. 2014, doi: 10.1007/s10470-014-0345-6.

[26] M. Atasoyu, H. Kuntman, B. Metin, N. Herencsar, and O. Cicekoglu, "Design of current-mode class 1 frequency-agile filter employing CDTAs," in *Proc. Eur. Conf. Circuit Theory Design (ECCTD)*, Aug. 2015, pp. 1–4, doi: 10.1109/ECCTD.2015.7300066.

[27] E. Alaybeyoğlu and H. Kuntman, "A new frequency agile filter structure employing CDTA for positioning systems and secure communications," *Anal. Integr. Circuits Signal Process.*, vol. 89, no. 3, pp. 693–703, Dec. 2016, doi: 10.1007/s10470-016-0770-9.

[28] D. Nand and N. Pandey, "New configuration for OFCC-based CM SIMO filter and its application as shadow filter," *Arabian J. Sci. Eng.*, vol. 43, no. 6, pp. 3011–3022, Jun. 2018, doi: 10.1007/s13369-017-3058-1.

[29] K. Chhabra, S. Singhal, and N. Pandey, "Realisation of CBTA based current mode frequency agile filter," in *Proc. 6th Int. Conf. Signal Process. Integr. Netw. (SPIN)*, Mar. 2019, pp. 1076–1081, doi: 10.1109/SPIN.2019.8711586.

[30] D. Singh and S. K. Paul, "Realization of current mode universal shadow filter," *AEU Int. J. Electron. Commun.*, vol. 117, Apr. 2020, Art. no. 153088, doi: 10.1016/j.aeue.2020.153088.

[31] D. Singh and S. K. Paul, "Improved current mode biquadratic shadow universal filter," *Informacije MIDEM*, vol. 52, no. 1, pp. 51–66, 2022, doi: 10.33180/InfMIDEM2022.106.

[32] R. Anurag, R. Pandey, N. Pandey, M. Singh, and M. Jain, "OTRA based shadow filters," in *Proc. Annu. IEEE India Conf. (INDICON)*, Dec. 2015, pp. 1–4, doi: 10.1109/INDICON.2015.7443524.

[33] M. T. Abuelma'atti and N. Almutairi, "New voltage-mode bandpass shadow filter," in *Proc. 13th Int. Multi-Conf. Syst., Signals Devices (SSD)*, Mar. 2016, pp. 412–415, doi: 10.1109/SSD.2016.7473695.

[34] M. T. Abuelma'atti and N. Almutairi, "New CFOA-based shadow banpass filter," in *Proc. Int. Conf. Electron., Inf., Commun. (ICEIC)*, Jan. 2016, pp. 1–3, doi: 10.1109/ELINFOCOM.2016.7562969.

[35] F. Khateb, W. Jaikla, T. Kulej, M. Kumngern, and D. Kubanek, "Shadow filters based on DDCC," *IET Circuits, Devices Syst.*, vol. 11, no. 6, pp. 631–637, 2017, doi: 10.1049/iet-cds.2016.0522.

[36] E. Alaybeyoğlu and H. Kuntman, "CMOS implementations of VDTA based frequency agile filters for encrypted communications," *Anal. Integr. Circuits Signal Process.*, vol. 89, no. 3, pp. 675–684, Dec. 2016, doi: 10.1007/s10470-016-0760-y.

[37] S. Buakaew, W. Narksarp, and C. Wongtaychatham, "Fully active and minimal shadow bandpass filter," in *Proc. Int. Conf. Eng., Appl. Sci., Technol. (ICEAST)*, Jul. 2018, pp. 1–4, doi: 10.1109/ICEAST.2018.8434448.

[38] S. Buakaew, W. Narksarp, and C. Wongtaychatham, "Shadow bandpass filter with *Q*-improvement," in *Proc. 5th Int. Conf. Eng., Appl. Sci. Technol. (ICEAST)*, Jul. 2019, pp. 1–4, doi: 10.1109/ICEAST.2019.8802535.

[39] S. Buakaew, W. Narksarp, and C. Wongtaychatham, "High quality-factor shadow bandpass filters with orthogonality to the characteristic frequency," in *Proc. 17th Int. Conf. Electr. Eng./Electron., Comput., Telecommun. Inf. Technol. (ECTI-CON)*, Jun. 2020, pp. 372–375, doi: 10.1109/ECTI-CON49241.2020.9158304.

[40] P. Moonmuang, T. Pukkalanun, and W. Tangsrirat, "Voltage differencing gain amplifier-based shadow filter: A comparison study," in *Proc. 6th Int. Conf. Eng., Appl. Sci. Technol. (ICEAST)*, Jul. 2020, pp. 1–4, doi: 10.1109/ICEAST50382.2020.9165352.

[41] S. Buakaew and C. Wongtaychatham, "Boosting the quality factor of the shadow bandpass filter," *J. Circuits, Syst. Comput.*, vol. 31, no. 14, Sep. 2022, Art. no. 2250248, doi: 10.1142/S0218126622502486.

[42] P. Huaihongthong, A. Chaichana, P. Suwanjan, S. Siripongdee, W. Sunthonkanokpong, P. Supavarasuwat, W. Jaikla, and F. Khateb, "Single-input multiple-output voltage-mode shadow filter based on VDDDAs," *AEU Int. J. Electron. Commun.*, vol. 103, pp. 13–23, May 2019, doi: 10.1016/j.aeue.2019.02.013.

[43] G. Varshney, N. Pandey, and R. Pandey, "Generalization of shadow filters in fractional domain," *Int. J. Circuit Theory Appl.*, vol. 49, no. 10, pp. 3248–3265, Oct. 2021, doi: 10.1002/cta.3054.

[44] S. D. Pathak, A. Luitel, S. Singh, and R. Pandey, "Second generation voltage conveyor II based shadow filter," in *Proc. 2nd Int. Conf. Emerg. Technol. (INCET)*, May 2021, pp. 1–5, doi: 10.1109/INCET51464.2021.9456370.

[45] N. Pandey and S. K. Paul, "Differential difference current conveyor transconductance amplifier: A new analog building block for signal processing," *J. Electr. Comput. Eng.*, vol. 2011, Jan. 2011, Art. no. 361384, doi: 10.1155/2011/361384.

[46] M. Kumngern, "DDTA and DDCCTA: New active elements for analog signal processing," in *Proc. IEEE Int. Conf. Electron. Design, Syst. Appl. (ICEDSA)*, Nov. 2012, pp. 141–145, doi: 10.1109/ICEDSA.2012.6507784.

[47] M. Kumngern, "CMOS differential difference voltage follower transconductance amplifier," in *Proc. IEEE Int. Circuits Syst. Symp. (ICSyS)*, Langkawi, Malaysia, Sep. 2015, pp. 133–136, doi: 10.1109/CircuitsAndSystems.2015.7394080.

[48] F. Khateb, M. Kumngern, T. Kulej, and D. Biolek, "0.5 V differential difference transconductance amplifier and its application in voltage-mode universal filter," *IEEE Access*, vol. 10, pp. 43209–43220, 2022, doi: 10.1109/ACCESS.2022.3167700.

[49] F. Khateb, M. Kumngern, T. Kulej, and D. Biolek, "0.3-volt rail-to-rail DDTA and its application in a universal filter and quadrature oscillator," *Sensors*, vol. 22, no. 7, p. 2655, Mar. 2022, doi: 10.3390/s22072655.

[50] M. Kumngern, P. Suksaibul, F. Khateb, and T. Kulej, "Electronically tunable universal filter and quadrature oscillator using low-voltage differential difference transconductance amplifiers," *IEEE Access*, vol. 10, pp. 68965–68980, 2022, doi: 10.1109/ACCESS.2022.3186435.

[51] F. Khateb, T. Kulej, M. Akbari, and M. Kumngern, "0.5-V high linear and wide tunable OTA for biomedical applications," *IEEE ACCESS*, vol. 9, pp. 103784–103794, 2021, doi: 10.1109/ACCESS.2021.3098183.

[52] F. Khateb, T. Kulej, M. Kumngern, and C. Psychalinos, "Multiple-input bulk-driven MOS transistor for low-voltage low-frequency applications," *Circuits, Syst., Signal Process.*, vol. 38, no. 6, pp. 2829–2845, Jun. 2019, doi: 10.1007/s00034-018-0999-x.

[53] F. Khateb, T. Kulej, M. Akbari, and K.-T. Tang, "A 0.5-V multiple-input bulk-driven OTA in 0.18-μm CMOS," *IEEE Trans. Very Large Scale Integr. (VLSI) Syst.*, vol. 30, no. 11, pp. 1739–1747, Nov. 2022, doi: 10.1109/TVLSI.2022.3203148.

[54] T. Tsukutani, M. Higashimura, N. Takahashi, Y. Sumi, and Y. Fukui, "Versatile voltage-mode active-only biquad with lossless and lossy integrator loop," *Int. J. Electron.*, vol. 88, no. 10, pp. 1093–1101, Oct. 2001, doi: 10.1080/00207210110071279.

FABIAN KHATEB received the M.Sc. and Ph.D. degrees in electrical engineering and communication and the M.Sc. and Ph.D. degrees in business and management from the Brno University of Technology, Czech Republic, in 2002, 2005, 2003, and 2007, respectively. He is currently a Professor with the Department of Microelectronics, Faculty of Electrical Engineering and Communication, Brno University of Technology; with the Department of Electrical Engineering, University of Defence, Brno; and also with the Department of Information and Communication Technology in Medicine, Faculty of Biomedical Engineering, Czech Technical University in Prague. He has authored or coauthored over 100 publications in journals and proceedings of international conferences. He holds five patents. He has expertise in new principles of designing low-voltage low-power analog circuits, particularly biomedical applications. He is a member of the editorial boards of *Microelectronics Journal*, *Sensors*, *Electronics*, and *Journal of Low Power Electronics and Applications*. He is an Associate Editor of IEEE Access, *Circuits, Systems and Signal Processing*, *IET Circuits, Devices and Systems*, and *International Journal of Electronics*. He was the Lead Guest Editor for the Special Issues on Low Voltage Integrated Circuits and Systems of *Circuits, Systems and Signal Processing*, in 2017; *IET Circuits Devices and Systems*, in 2018; and *Microelectronics Journal*, in 2019. He was also a Guest Editor for the Special Issue on Current-Mode Circuits and Systems; Recent Advances, Design and Applications of *International Journal of Electronics and Communications*, in 2017.

MONTREE KUMNGERN received the B.S.Ind.Ed. degree from the King Mongkut's University of Technology Thonburi, Thailand, in 1998, and the M.Eng. and D.Eng. degrees from the King Mongkut's Institute of Technology Ladkrabang, Thailand, in 2002 and 2006, respectively, all in electrical engineering. In 2007, he was a Lecturer with Department of Telecommunications Engineering, Faculty of Engineering, King Mongkut's Institute of Technology Ladkrabang. From 2010 to 2017, he was an Assistant Professor and he is currently an Associate Professor. He has authored or coauthored over 200 publications in journals and proceedings of international conferences. His research interests include analog and digital integrated circuits, discrete-time analog filters, non-linear circuits, data converters, and ultra-low voltage building blocks for biomedical applications.

TOMASZ KULEJ received the M.Sc. and Ph.D. degrees from the Gdańsk University of Technology, Gdańsk, Poland, in 1990 and 1996, respectively. He was a Senior Design Analysis Engineer with Polish branch of Chipworks Inc., Ottawa, Canada. He is currently an Associate Professor with the Department of Electrical Engineering, Częstochowa University of Technology, Poland, where he conducts lectures on electronics fundamentals, analog circuits, and computer aided design. He has authored or coauthored over 90 publications in peer-reviewed journals and conferences. He holds three patents. His recent research interest includes analog integrated circuits in CMOS technology, with an emphasis to low voltage and low power solutions. He is an Associate Editor of the *Circuits Systems and Signal Processing* and *IET Circuits Devices and Systems*. He was also the Guest Editor for the Special Issues on Low Voltage Integrated Circuits of *Circuits Systems and Signal Processing*, in 2017; *IET Circuits Devices and Systems*, in 2018; and *Microelectronics Journal*, in 2019.

RAJEEV KUMAR RANJAN (Senior Member, IEEE) was born in India, in 1979. He received the M.Tech. and Ph.D. degrees from IIT (ISM) Dhanbad, India, in 2007 and 2016, respectively. He is currently an Assistant Professor with the Department of Electronics Engineering, IIT (ISM) Dhanbad. He has authored more than 34 articles in esteemed journals and more than 34 papers in esteemed conferences. His main research interests include communication and VLSI signal processing circuits and systems.